Journal of the Ceramic Society of Japan 125 [11] 829-832 2017 Full paper

Valency effects of cation dopant on ultraphosphate glass electrolytes for intermediate temperature fuel cells

Hirofumi SUMI†

Inorganic Functional Materials Research Institute, National Institute of Advanced Industrial Science and Technology, Nagoya 463–8560, Japan

Some solid phosphates show high protonic conductivity in the intermediate temperature range at 150–250°C. Although the conductivity of crystalline phosphate materials, such as CsH_2PO_4 and $CsHSO_3$, is high at intermediate temperature, it decreases significantly below phase transition temperature. In order to quench the structure of the high temperature phase with high conductivity, non-crystalline ultraphosphate glasses without phase transition in the wide temperature range at 25–250°C were evaluated. In the present work, the valency effects of cation dopant on protonic conductivity and glass structure were investigated. The P–O bonding was strengthened by doping trivalent La, which decreased proton conductivity. On the other hand, orthophosphate and end phosphate structures were formed by doping univalent Cs. The conductivity of $30Cs_2O–70P_2O_5$ glass was 1.7×10^{-3} S/cm at 200°C. However, the production of free orthophosphoric acid deteriorated the chemical stability for Cs-doped phosphate glasses. The $30ZnO–70P_2O_5$ glass has a potential as an electrolyte of intermediate temperature fuel cells, since a maximum power density of 1.2 mW/cm^2 was obtained at 200°C.

Key-words : Phosphate glass, Intermediate temperature fuel cell, Proton conduction, Raman spectroscopy, Magic angle spinning-nuclear magnetic resonance (MAS-NMR)

[Received June 9, 2017; Accepted August 25, 2017]

1. Introduction

Approximately several thousand units of phosphoric acid fuel cell (PAFC) systems have been installed since 1970s. PAFC systems are generally operated at ca. 200°C, and their power generation efficiency is more than 40%. The electrolyte of orthophosphoric acid (H_3PO_4) is retained in a SiC matrix of 0.1–0.2 mm in thickness. It is necessary to refill the electrolyte due to possible liquid loss. The electrical interconnector is composed of multilayers with dense and porous structures. The dense layers separate fuel and air in PAFC stacks, and the porous layers reserve phosphoric acid, i.e. a refill for the electrolyte losses realizes more than 40000 h durability.[1] However, the reduction in cost is not expected to be below US$3000/kW for 100–1000 kW-class PAFC systems.[2),3] Most observers believe that the target cost must be reduced to around US$1000/kW for initial market entry, falling to below US$500/kW with volume production.[4),5] Therefore, it is difficult to realize small-scale PAFC systems below 100 kW.

On the other hand, more than 150 thousand units of residential micro combined heat and power (CHP) polymer electrolyte fuel cell (PEFC) systems have been installed by 2015 in Japan. The rated electrical power is 700 W for the residential micro CHP systems. Perfluorosulfonic polymer membranes are generally used as electrolytes. The operating temperature of PEFC is below 80°C, because humidification is required to obtain protonic conductivity.[6),7] The low temperature operation requires a large amount of expensive platinum catalysts to obtain sufficient electrode activity.

Sulfonated or phosphoric acid-doped hydrocarbon polymers have been developed for electrolytes of intermediate temperature (150–300°C) fuel cells. For example, the conductivity of H_3PO_4-doped poly(benzimidazole) (PBI) was 6.8×10^{-2} S/cm at 200°C and 5% relative humidity.[8] However, phosphoric acid is easily desorbed from PBI above 150°C.[9] On the other hand, some crystalline inorganic materials also show high protonic conductivity. The conductivity of CsH_2PO_4[10),11] and $CsHSO_3$[12] are 1×10^{-2} S/cm at 250°C and 8×10^{-2} S/cm at 200°C, respectively. However, a phase transition occurs at 230 and 140°C for the crystalline CsH_2PO_4 and $CsHSO_3$, respectively, which causes a significant decrease in protonic conductivity at low temperature. Hybridization to other inorganic materials has been attempted in order to decrease the effect of the phase transition.[13)–15]

Abe et al.[16),17] previously discovered protonic conductivity for non-crystalline phosphate glasses. Water exists as a hydroxyl (OH) group in general glasses. The hydrogen bonding is strong in phosphate glasses, which means the weakening of O–H bonding and the enhancement of proton mobility.[18] In the previous work,[19),20] the protonic conductivity of ultraphosphate glasses with different divalent cations was compared. The short-range order of the 30 mL%MO–70 mol%P_2O_5 (M = Zn, Ba) glasses was based on middle phosphate (Q_P^2) structure. In $BaO–P_2O_5$ glasses melt at 800°C, branching phosphate (Q_P^3) structure was also contained, and their conductivity was only 2×10^{-5} S/cm at 250°C. On the other hand, $ZnO–P_2O_5$ glasses had orthophosphate (Q_P^0) and end phosphate (Q_P^1) structures, which enhanced mobile proton concentration. The protonic conductivity of $ZnO–P_2O_5$ glasses was 1×10^{-3} S/cm at 250°C.[19] The conductivity was dependent on melting temperature.[19)–21] Furthermore, $WO_3–P_2O_5$-based glasses also have high protonic conductivity at intermediate temperature.[22),23] In the present work, the protonic conductivity of $MO–P_2O_5$ ($M = Cs^+$, Zn^{2+}, La^{3+}) glasses and the characteristics of H_2/O_2 fuel cells with $Cs_2O–P_2O_5$ and $ZnO–P_2O_5$ glass electrolytes were evaluated. The valency effects of

† Corresponding author: H. Sumi; E-mail: h-sumi@aist.go.jp

DOI http://doi.org/10.2109/jcersj2.17129

cation dopant on glass structure was investigated with magic angle spinning-nuclear magnetic resonance (MAS-NMR) and Raman spectroscopy for ultraphosphate glasses.

2. Experimental

Ultraphosphate glasses of $(30-x)$ZnO–x*M*O–70P_2O_5 [M = $2Cs^+$ (x = 10, 30), Zn^{2+}, $2/3La^{3+}$ (x = 5)] were prepared by a conventional melt-quenching technique under an ambient condition. The powders of ZnO, La_2O_3 and Cs_2CO_3 were mixed with H_3PO_4 (85% liquid) with adding the proper amount of water. The resulting slurry was stirred and dried in a polytetrafluoroethylene beaker at 200°C overnight. The product was melted in a platinum crucible for 30 min at 800°C. The melt was poured on a stainless steel plate and subsequently pressed by another one. For M = $2/3La^{3+}$ and $x \geq 10$, the product could not be melt at 800°C. The clear disc-shaped glasses of 1.8 mm in thickness were obtained. The products were confirmed to be non-crystalline solids by X-ray diffraction.

The protonic conductivity was evaluated by a four-terminal AC impedance measurement with an impedance analyzer (Solartron Analytical 1455A) at 100–250°C. Au electrodes of 6 mm in diameter were formed by evaporation on both surfaces of the disc-shaped glass samples. AC impedance was measured between the anode and the cathode under the OCV state in the frequency range of 1 MHz to 0.1 Hz with 20 steps per logarithmic decade. The conductivities were measured at 100, 150, 200 and 250°C with a supply of nitrogen gas humidified at room temperature (P_{H_2O} = 0.03 atm). The characteristics of fuel cells were measured with a potentiostat/galvanostat (Solartron Analytical 1470E) at 200°C from open circuit voltage (OCV) to a half of OCV at a sweep rate of 5 mV s^{-1} to evaluate the maximum power density. Air and 20%H_2–N_2 humidified at room temperature (p_{H_2O} = 0.03 atm) were supplied to the cathode and anode, respectively, at a flow rate of 100 mL/min. Carbon papers with Pt loading of 0.5 mg/cm^2 (ElectroChem Inc. EC-10-05-7) were used as electrodes. The Pt/C electrodes of 1 cm square were pasted on the both surfaces of the disc-shaped glass electrolyte of 1.8 mm in thickness by hot-pressing.

The glass structures were evaluated by Raman spectroscopy and MAS-NMR. The Raman spectra were measured at room temperature with a green diode laser of 532 nm wavelength on a Horiba XploRA. The ^1H and ^{31}P MAS-NMR spectra were measured at room temperature with a Varian INOVA-300 spectrometer using a Doty probe. The glass powders were placed in a Si_3N_4 rotor of 7 mm in diameter with polyimide resin caps. The Larmor frequencies were 300 and 121 MHz at 7.05 T for ^1H and ^{31}P, respectively. The spinning rate of the sample was 7 kHz. The $\pi/2$ pulse length for the ^1H and ^{31}P nuclei was 5.2 µs with a 60 s of recycle delay.

3. Results and discussion

Figure 1 shows the protonic conductivity in a steam partial pressure of 0.03 atm for $(30-x)$ZnO–x*M*O–70P_2O_5 (M = $2Cs^+$, Zn^{2+}, $2/3La^{3+}$) glasses melted at 800°C. The protonic conductivity adheres to the following sequence in the temperature range of 100–250°C: M = $2/3La^{3+}$ (x = 5) < M = Zn^{2+} < M = $2Cs^+$ (x = 10) < M = $2Cs^+$ (x = 30). The conductivity of 30Cs_2O–70P_2O_5 glass was 1.7 × 10^{-3} S/cm at 200°C, which was 7 times higher than that of 30ZnO–70P_2O_5 glass. The protonic conductivity showed Arrhenius dependence on temperature. The activation energy derived from the slope of Arrhenius plots for M = $2/3La^{3+}$ was 0.83 eV, which was larger than that for M = $2Cs^+$ (0.52 eV) and Zn^{2+} (0.56 eV). The protonic conductivities of

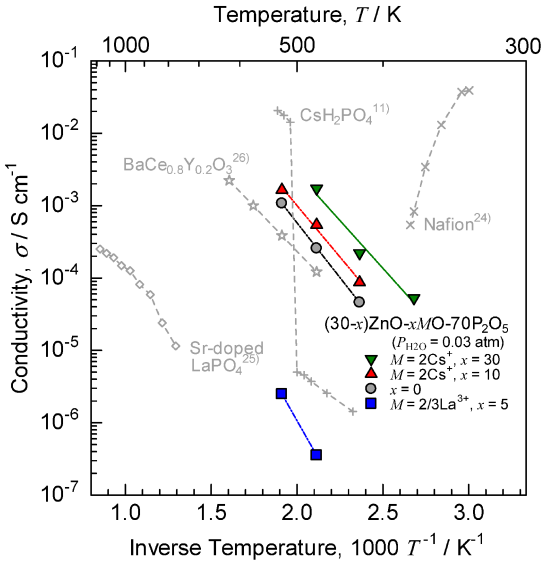

Fig. 1. Protonic conductivity in a steam partial pressure of 0.03 atm for $(30-x)$ZnO–x*M*O–70P_2O_5 (M = $2Cs^+$, Zn^{2+}, $2/3La^{3+}$) glasses melted at 800°C, Nafion,[24] CsH_2PO_4,[11] Sr-doped $LaPO_4$[25] and $BaCe_{0.8}Y_{0.2}O_3$.[26]

Nafion,[24] CsH_2PO_4,[11] Sr-doped $LaPO_4$[25] and $BaCe_{0.8}Y_{0.2}O_3$[26] are also shown in Fig. 1. The activation energies for M = $2Cs^+$ and $2/3La^{3+}$ were almost the same as that for high temperature phases of CsH_2PO_4 and $LaPO_4$, respectively. For the crystalline CsH_2PO_4, the phase transition occurred at 230°C, which causes a significantly decrease in protonic conductivity at low temperature. For non-crystalline 30Cs_2O–70P_2O_5 glass, no phase transition occurred in the wide temperature range at 25–250°C. It is believed that the structure of the high temperature phase with high protonic conductivity might be quenched in the short-range order of the ultraphosphate glasses. The conductivities of $(30-x)$ZnO–$x$$Cs_2O$–70$P_2O_5$ glasses were higher than that of proton conductive ceramics of $BaCe_{0.8}Y_{0.2}O_3$[26] at 200 and 250°C. On the other hand, the protonic conductivity was low for M = $2/3La^{3+}$ because of the increase in melting point. The thermal stability was improved by doping with La. It was reported that LaP_3O_9 glass was chemically stable at 850°C, and the conductivity was ca. 10^{-4} S/cm at 700°C.[27]

Figure 2 shows the current–voltage and power characteristics at 200°C for the fuel cell using 30Cs_2O–70P_2O_5 and 30ZnO–70P_2O_5 glass electrolytes of 1.8 mm in thickness melted at 800°C. The maximum power density was 1.2 mW/cm^2 at 200°C for the fuel cell with the 30ZnO–70P_2O_5 glass electrolyte melted at 800°C. However, the power density was only 0.18 mW/cm^2 at 200°C for the fuel cell with the 30Cs_2O–70P_2O_5 glass electrolyte in spite of higher protonic conductivity than 30ZnO–70P_2O_5. The OCVs were 0.76 and 0.58 V for 30ZnO–70P_2O_5 and 30Cs_2O–70P_2O_5, respectively, which were lower than theoretical electromotive force. After testing, the deformation of the glass electrolytes was confirmed around the gas sealant, which caused the decrease in OCVs. This suggests that the glass transition temperature of 30Cs_2O–70P_2O_5 is lower than that of 30ZnO–70P_2O_5. Unfortunately, the glass transition temperature of the ultraphosphate glasses could not be determined by thermogravimetric-differential thermal analysis (TG–DTA) in an ambient air atmosphere in the present work, because a large amount of water was desorbed from the phosphate glasses near the glass transition temperature. In the future, the author would like to evaluate the

glass transition temperature by TG–DTA under atmospheric control, and to investigate the improvement of chemical stability of the ultraphosphate glasses.

The glass structure was investigated to consider the association with protonic conductivity and chemical stability. **Figure 3** shows the Raman spectra for $(30-x)$ZnO–x*M*O–70P_2O_5 ($M = 2Cs^+$, Zn^{2+}, $2/3La^{3+}$) glasses melted at 800°C. The peak intensity is normalized by the peak at ~700 cm^{-1}. The Raman spectra are similar to the spectra of zinc phosphate glasses reported by Brow et al.[28] The Raman peaks at ~700, 900, 1000, 1150 and 1300 cm^{-1} were ascribed to the bonding of straight-chain (O–P–O), PO_4 (Q_P^0), PO_3 (Q_P^1), PO_2 (Q_P^2), and P=O, respectively. The intensity of PO_2 peak adheres to the following sequence: $M = 2Cs^+ < Zn^{2+} < 2/3La^{3+}$. The side-chain P–O bonding was strengthened by substituting divalent Zn^{2+} ion with trivalent La^{3+} ion. The O–P–O peak for $M = 2Cs^+$ shifted to lower wave number compared to those for $M = Zn^{2+}$ and $2/3La^{3+}$, suggesting that the P–O interionic distance increased by substituting divalent Zn^{2+} ion with univalent Cs^+ ion. On the other hand, Romain and Novak[29] reported the Raman spectra of crystalline CsH_2PO_4. The spectrum shape of 30Cs_2O–70P_2O_5 glass is similar to that of CsH_2PO_4 at 246°C, which shows high protonic conductivity. The Raman peaks of 30Cs_2O–70P_2O_5 glass were shifted to higher wave number compared to CsH_2PO_4 at 246°C, which might be caused by the difference in the P–O interionic distance.

Figure 4(a) shows the ^{31}P MAS-NMR spectra for $(30-x)$-ZnO–x*M*O–70P_2O_5 ($M = 2Cs^+$, Zn^{2+}, $2/3La^{3+}$) glasses melted at 800°C. The short-range order of the ultraphosphate glasses was based on middle phosphate structure, because the area of the Q_P^2 peak at $\delta \sim -30$ ppm was the largest among the all peaks. The shoulder Q_P^3 peak was observed at $\delta \sim -40$ ppm for 25ZnO–5$La_{2/3}O$–70P_2O_5 glass. It was previously reported for 30BaO–70P_2O_5 glasses that the Q_P^3 structure became a potential barrier

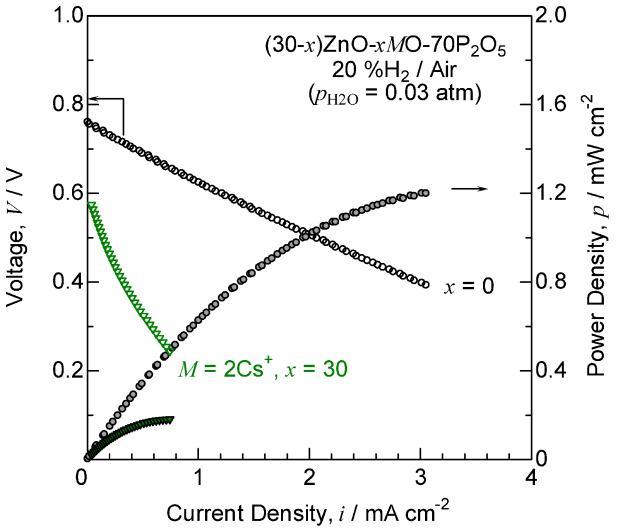

Fig. 2. Current–voltage and power characteristics at 200°C for the fuel cell using Pt/C electrodes and 30Cs_2O–70P_2O_5 and 30ZnO–70P_2O_5 glass electrolytes of 1.8 mm in thickness melted at 800°C. Air and 20%H_2–N_2 humidified at room temperature ($p_{H_2O} = 0.03$ atm) were supplied to the cathode and anode, respectively.

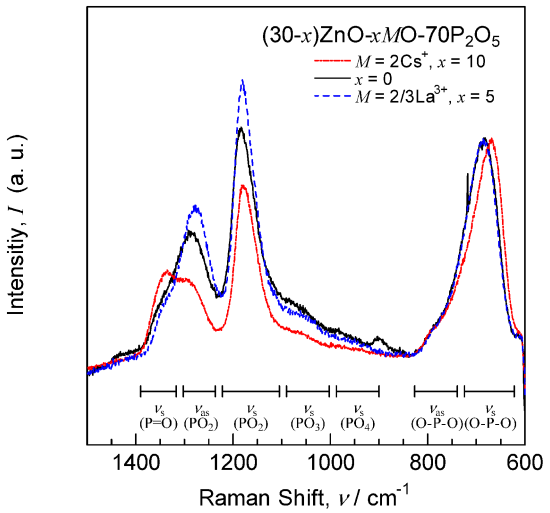

Fig. 3. Raman spectra for $(30-x)$ZnO–x*M*O–70P_2O_5 ($M = 2Cs^+$, Zn^{2+}, $2/3La^{3+}$) glasses melted at 800°C. The peak intensity is normalized by the peak at ~700 cm^{-1}.

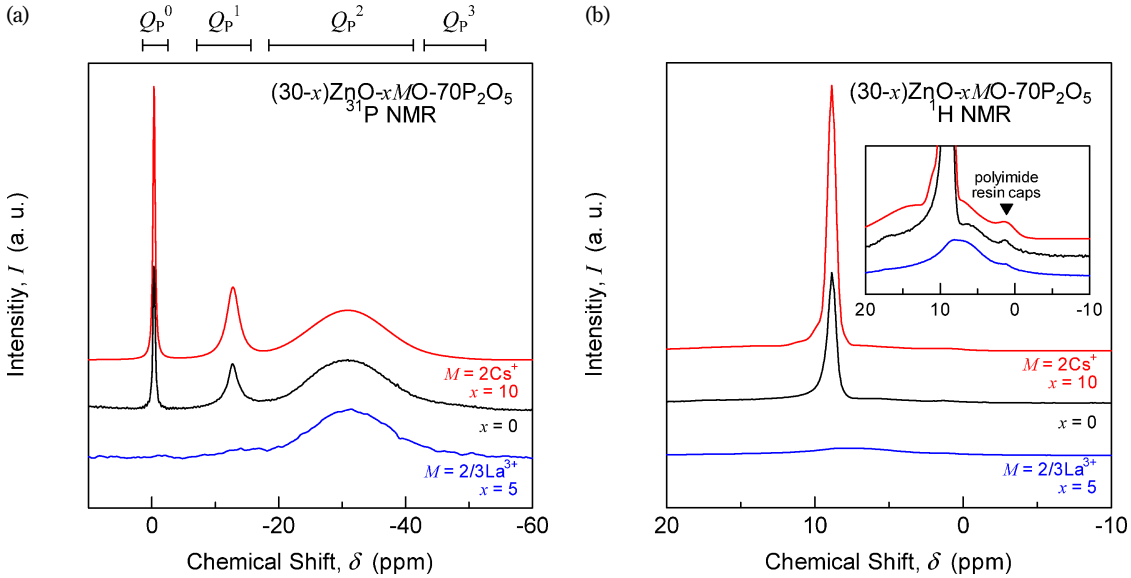

Fig. 4. (a) ^{31}P and (b) ^{1}H MAS-NMR spectra for $(30-x)$ZnO–x*M*O–70P_2O_5 ($M = 2Cs^+$, Zn^{2+}, $2/3La^{3+}$) glasses melted at 800°C.

for proton conduction.[19] On the other hand, the intensities of the $Q_P{}^0$ at $\delta \sim 0$ ppm and $Q_P{}^1$ peaks at $\delta \sim -12$ ppm were strong for $M = 2Cs^+$ and Zn^{2+}. The terminal nonbridging oxygens bind doping cations or protons to keep an electroneutral state in the glasses. The increase in the nonbridging oxygens enhances proton concentration in ultraphosphate glasses. However, the intensity of the $Q_P{}^0$ peak was too strong for $M = 2Cs^+$ due to the production of free orthophosphoric acid by the further breakage of P–O bonding, which decreased the chemical stability. The ^{1}H MAS-NMR spectra are shown in Fig. 4(b). Small peaks appeared at $\delta \sim 1$ ppm from a polyimide resin caps of the rotor. The broad peak was detected at $\delta \sim 6$ ppm for the all samples as shown in the inset of Fig. 4(b), which was ascribed to OH group in the phosphate glasses. The broad peak positions were almost comparable for $M = 2Cs^+$, Zn^{2+} and $2/3La^{3+}$. Abe et al.[17] reported that the mobile proton concentration of metaphosphate glasses was ca. 1 mol/L estimated by Fourier transform-infrared spectroscopy (FT-IR). However, the protonic conductivity was expected to be less than 10^{-6} S/cm at 144°C. They suggested that a large amount of molecular water should be introduced into the phosphate glasses to improve the protonic conductivity.[30] In the present work, the melting temperature of ultraphosphate glasses was decreased to 800°C to retain a large amount of water in the glasses. For $M = 2Cs^+$ and Zn^{2+}, the sharp peak was observed at $\delta \sim 9$ ppm. It has been reported that the peak appeared at lower magnetic field, when the hydrogen bonding was strengthened.[31] The mobile proton concentration of $30ZnO–70P_2O_5$ glass was estimated to be ca. 5×10^3 mol/L by FT-IR.[20] The sharp peak also observed for crystalline CsH_2PO_4 at 252°C,[32] which shows high protonic conductivity. The $10Cs_2O–20ZnO–70P_2O_5$ glass is expected to have a large amount of 'mobile' protons due to the appearance of the significantly strong ^{1}H NMR peak at $\delta \sim 9$ ppm, which realized high protonic conductivity.

4. Conclusion

In the present work, the valency effects of cation dopant on protonic conductivity and glass structure were investigated for $(30 - x)ZnO–xMO–70P_2O_5$ ($M = Cs^+$, Zn^{2+}, La^{3+}) glasses. The protonic conductivity adheres to the following sequence in the temperature range of 100–250°C: $M = 2/3La^{3+} < Zn^{2+} < 2Cs^+$. The short-range order of the ultraphosphate glasses melted at 800°C was based on middle phosphate ($Q_P{}^2$) structure. The $25ZnO–5La_{2/3}O–70P_2O_5$ glass partially contained branching phosphate ($Q_P{}^3$) structure due to the strengthening of the side-chain P–O bonding by substituting divalent Zn^{2+} ion with trivalent La^{3+} ion. The $10Cs_2O–20ZnO–70P_2O_5$ glasses have orthophosphate ($Q_P{}^0$) and end phosphate ($Q_P{}^1$) structures due to the increase in the P–O interionic distance increased by substituting divalent Zn^{2+} ion with univalent Cs^+ ion, which enhanced mobile proton concentration. The conductivity of $30Cs_2O–70P_2O_5$ glass was 1.7×10^{-3} S/cm at 200°C. However, the production of free orthophosphoric acid deteriorated the chemical stability of $30Cs_2O–70P_2O_5$ glasses. The maximum power density of 1.2 mW/cm^2 was obtained at 200°C for the H_2/O_2 fuel cells using $30ZnO–70P_2O_5$ glass electrolyte of 1.8 mm in thickness.

Acknowledgments The author would like to dedicate this paper to the memory of Professor Yoshihiro Abe, Nagoya Institute of Technology, who passed away in February 6th, 2017. He discussed proton conductive ultraphosphate glasses with me frequently since 2002. The author would like to thank Professor Toshihiro Kasuga, Nagoya Institute of Technology, for his valuable advice. The author is grateful to Dr. Masakazu Nishida, Senior researcher of National Institute of Advanced Industrial Science and Technology, for his help in the MAS-NMR measurement. This work was supported by Japan Society for the Promotion of Science (JSPS) KAKENHI Grants-in-Aid of for Young Scientists No. 25871187.

References

1) N. Sammes, R. Bove and K. Stahl, *Curr. Opin. Solid St. M.*, **8**, 372–378 (2004).
2) R. Anahara, *J. Power Sources*, **49**, xi–xiv (1994).
3) J. Whitaker, *J. Power Sources*, **71**, 71–74 (1998).
4) G. MacKerron, *J. Power Sources*, **86**, 28–33 (2000).
5) B. C. H. Steele, *Nature*, **414**, 345–352 (2001).
6) Y. Sone, P. Ekdunge and D. Simonsson, *J. Electroanal. Chem.*, **143**, 1254–1259 (1996).
7) K. D. Kreuer, Th. Dippel, N. G. Hainovsky and J. Maier, *Berich. Bunsen Gesell.*, **96**, 1736–1742 (1992).
8) R. He, Q. Li, G. Xiao and N. J. Bjerrum, *J. Membrane Sci.*, **226**, 169–184 (2003).
9) G. Liu, H. Zhang, J. Hu, Y. Zhai, D. Xu and Z. Shao, *J. Power Sources*, **162**, 547–552 (2006).
10) D. A. Boysen, T. Uda, C. R. I. Chisholm and S. M. Haile, *Science*, **303**, 68–70 (2004).
11) J. Otomo, N. Minagawa, C. Wen, K. Eguchi and H. Takahashi, *Solid State Ionics*, **156**, 357–369 (2003).
12) S. M. Haile, D. A. Boysen, C. R. I. Chisholm and R. B. Merle, *Nature*, **410**, 910–913 (2001).
13) T. Matsui, T. Kukino, R. Kikuchi and K. Eguchi, *Electrochem Solid St.*, **8**, A256–A258 (2005).
14) T. Matsui, T. Kukino, R. Kikuchi and K. Eguchi, *J. Electrochem. Soc.*, **153**, A339–A342 (2006).
15) H. Muroyama, T. Matsui, R. Kikuchi and K. Eguchi, *J. Electrochem. Soc.*, **153**, A1077–A1080 (2006).
16) Y. Abe, H. Shimakawa and L. L. Hench, *J. Non-Cryst. Solids*, **51**, 357–365 (1982).
17) Y. Abe, H. Hosono, Y. Ohta and L. L. Hench, *Phys. Rev. B*, **38**, 10166–10169 (1998).
18) H. Sumi, M. Mizutani, M. Takahashi, M. Hayashi, T. Iwamoto, M. Sakurai, M. Watanabe and Y. Abe, *Electrochemistry*, **72**, 633–636 (2004).
19) H. Sumi, Y. Nakano, Y. Fujishiro and T. Kasuga, *Int. J. Hydrogen Energ.*, **38**, 15354–15360 (2013).
20) H. Sumi, Y. Nakano, Y. Fujishiro and T. Kasuga, *Solid State Sci.*, **45**, 5–8 (2015).
21) H. Takahashi, A. Shimizu and T. Sakuma, *J. Phys. Soc. Jpn.*, **79**, 115–117 (2010).
22) H. Sumi, M. Mizutani, M. Takahashi, M. Sakurai, M. Watanabe and Y. Abe, *Electrochemistry*, **73**, 194–198 (2005).
23) T. Ishiyama, S. Suzuki, J. Nishii, T. Yamashita, H. Kawazoe and T. Omata, *Solid State Ionics*, **262**, 856–859 (2014).
24) J. J. Sumner, S. E. Creager, J. J. Ma and D. D. DesMarteau, *J. Electrochem. Soc.*, **145**, 107–110 (1998).
25) K. Amezawa, H. Maekawa, Y. Tomii and N. Yamamoto, *Solid State Ionics*, **145**, 233–240 (2001).
26) K. D. Kreuer, *Solid State Ionics*, **97**, 1–15 (1997).
27) K. Amezawa, T. Tomiga, N. Yamamoto, T. Hanada and Y. Tomii, *J. Am. Ceram. Soc.*, **88**, 3211–3214 (2005).
28) R. K. Brow, D. R. Tallant, S. T. Myers and C. C. Phifer, *J. Non-Cryst. Solids*, **191**, 45–55 (1995).
29) F. Romain and A. Novak, *J. Mol. Struct.*, **263**, 69–74 (1991).
30) Y. Abe, G. Li, M. Nogami and T. Kasuga, *J. Electrochem. Soc.*, **143**, 144–147 (1996).
31) Y. Sato, Y. Shen, M. Nishida, W. Kanematsu and T. Hibino, *J. Mater. Chem.*, **22**, 3973–3981 (2012).
32) G. Kim, F. Blanc, Y.-Y. Hu and C. P. Grey, *J. Phys. Chem. C*, **117**, 6504–6515 (2013).